

Optimizing Camera Configurations for Multi-View Pedestrian Detection

Yunzhong Hou[†] Xingjian Leng[†]

[†] Australian National University
 {firstname.lastname}@anu.edu.au

Tom Gedeon[‡] Liang Zheng[†]

[‡] Curtin University
 {firstname.lastname}@curtin.edu.au

Abstract

Jointly considering multiple camera views (multi-view) is very effective for pedestrian detection under occlusion. For such multi-view systems, it is critical to have well-designed camera configurations, including camera locations, directions, and fields-of-view (FoVs). Usually, these configurations are crafted based on human experience or heuristics. In this work, we present a novel solution that features a transformer-based camera configuration generator. Using reinforcement learning, this generator autonomously explores vast combinations within the action space and searches for configurations that give the highest detection accuracy according to the training dataset. The generator learns advanced techniques like maximizing coverage, minimizing occlusion, and promoting collaboration. Across multiple simulation scenarios, the configurations generated by our transformer-based model consistently outperform random search, heuristic-based methods, and configurations designed by human experts, shedding light on future camera layout optimization.

1. Introduction

Multiple camera views (multi-view) are becoming more and more popular for machine understanding. Unlike a monocular view (only one camera), multi-view systems can jointly consider different cameras at different angles to address challenges in recognition including ambiguities, occlusions, and limited field-of-view (FoV) coverage. To mention a few examples, multi-view classification [40, 48] uses circular or spherical camera rigs to capture an object from diverse angles and reduce ambiguities; multi-view stereo [45, 57] recovers the 3D shape from a collection of 2D images; autonomous vehicles [4, 25, 32] and multi-camera tracking [23, 42] expands the FoV coverage with multiple cameras. In this work, we focus on multi-view pedestrian detection [7, 22], a specific usage of multi-view systems that use multiple cameras to jointly combat occlusions, reduce ambiguities, increase FoV coverage, and ultimately locate pedestri-



(a) Camera views given by a human expert (top) and our method (bottom).



(b) FoV coverage from a human expert (left) vs. our search method (right). Less blue colors indicate the area being covered by more cameras. Zoom in to see the ground truth pedestrian locations (orange dots) and detection results (heatmap overlay).

Figure 1. Comparison between human expert design and searched configuration. On the test set of this scenario, these two configurations achieve 69.9% and 91.9% MODA, respectively.

ans in 3D from a bird's-eye-view (BEV).

For these multi-view systems, camera configurations including locations, directions, and FoVs are critical parameters. Poor camera configurations can impact overall system performance and are very difficult to remedy with image processing tools like CNNs, since the content in images may already be limited.

Usually, camera configurations are determined by human experts or based on heuristics. On the one hand, *experts* design the configurations based on experience [60] or general guidelines [10, 20, 54]. Unfortunately, these designs are usually directly adopted without further validation. On the other hand, *heuristic-based methods* focus on the FoV coverage and study camera placements that ensure each location on building floor plans is covered by at least one camera [13, 14]. However, these methods do not consider dynamic

occlusions from foreground objects such as pedestrians or vehicles, and more importantly, the image processing step (*e.g.*, object detection). In fact, neither of these existing solutions can guarantee the overall system performance for their configurations.

In this paper, we aim to directly optimize the camera configurations with the final multi-view pedestrian detection accuracy as the objective. Unlike previous approaches that either rely on human experience [20, 60] or the heuristic of FoV coverage [14], the proposed optimization is directed by quantitative analysis, while taking both dynamic occlusions and the pedestrian detection network into account. In Fig. 1, we demonstrate some human expert designs and compare them with our searched configurations. Compared to the human expert configurations, the searched results are more creative with the camera positioning, and can find views with less obstruction yet more collaboration and overlapping FoV. Thus, even with the same pedestrian detector, the proposed configuration provides more advantages than expert settings.

To study this problem, we formulate the camera configuration search as an interactive process between an **agent** who can predict camera configurations, and an **environment** that takes the predicted configurations and returns the pedestrian detection accuracy as their efficacy. Specifically, we first build the *interactive environment*. By connecting the Carla [12] simulation engine for autonomous vehicles and existing multi-view pedestrian detection networks, we introduce CarlaX, an interactive playground that can render camera views from given configurations and return the detection accuracy of specific multi-view pedestrian detectors as feedback. We then introduce a novel *camera configuration generator* as the agent. Using a transformer sequence predictor, the network generates the location, direction, and FoV for the next camera, iteratively. Importantly, to navigate through the non-differentiable parts¹ while sufficiently exploring the vast combinations², we introduce a reinforcement-learning-based *training scheme* to effectively search the configuration space while jointly training the multi-view detection network. We also introduce two differentiable regularization terms to make the reinforcement learning search process more effective.

Across multiple scenarios, our approach proves consistently advantageous over random search, heuristic-based methods, and human expert design. We will make the CarlaX playground and the code for our approach publically available to promote future work on smart vision, and to incentivize the community to include more into optimization aside from neural network parameters.

¹Interaction with the simulation engine, rendering, *etc.*

²For a 20×20 m² square with camera height from 0 to 4 m, quantizing the spatial resolution by 0.1 m would give 1.6 million combinations. Note that camera rotations and FoV are yet to be factored in, and we have to do this for all N cameras.

Overall, our contributions are as listed follows,

- a simulation environment for camera configuration study,
- a transformer-based camera configuration generator, and
- a reinforcement-learning-based training scheme that supports joint training for the detection network.

2. Related Work

Multi-view pedestrian detection aims to detect pedestrians from a bird’s-eye-view (BEV) under heavy occlusion, by jointly considering multiple camera views. Some [3, 8] merge the multi-view anchor box feature to provide the overall scenario description. Others [21, 22, 47] use the anchor-free approach and directly project image feature maps to BEV using camera tomography. In this work, we take MVDet architecture [22] as the multi-view detector.

Camera placement optimization. A closely related line of work in computational geometry is the Art Gallery Problem [38, 55], which aims to *maximize the FoV coverage*, and find the optimal camera locations that ensure each point on the building floor plan is visible and tries to minimize the number of cameras required [13, 14]. Specifically, Sun *et al.* [49] investigate a learning-based camera placement method. However, in our study, we find there are many solutions that satisfy maximal coverage, but unlike our method, that directly optimizes for detection accuracy, such solutions often fail to produce the best detection results in complex scenes with occluded targets.

Some also try to optimize the camera placements for *better task performance*. MVTN [18] uses a 3D point cloud as initial input and then estimates the best camera layout for each different object. Recently, Hou *et al.* [24] investigate how to select the most helpful views in multi-view systems for the best efficiency. A concurrent work by Klinghoffer *et al.* [30] also investigates camera placement. However, their experiments on stereo depth estimation and autonomous vehicles are at much smaller scales (<10 m³) compared to this work (>1000 m³).

For *3D reconstruction*, researchers in active vision study a very similar problem of view planning where the location of 3D sensors are determined for 3D reconstructions [9, 15]. View planning is also investigated in UAV reconstruction to maximize the constructability while minimizing the flight time [33, 58]. Lee *et al.* [31] focus on NeRF [35] and find the best views to improve a coarse model. However, such methods often require hundreds of images to fully reconstruct a scenario and usually reconstruct static objects or buildings, whereas multi-view pedestrian detection usually jointly considers fewer than ten cameras due to GPU hardware constraints and focuses on moving pedestrians.

Other study on camera hardware. Over the years, researchers include more components in the imaging process into optimization, including sensor multiplexing for image quality [5], phase-coded aperture [17] and focal length [19]

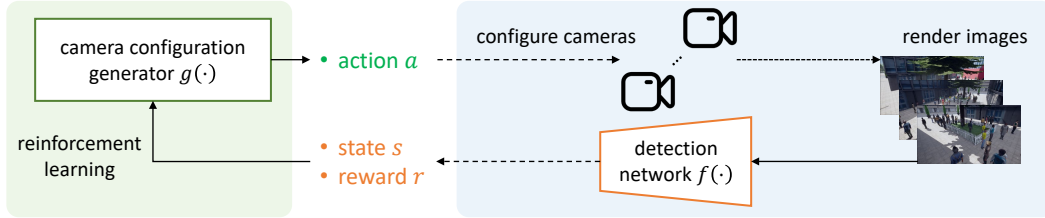


Figure 2. Overview of the proposed optimization method for camera configuration. On the left, the agent (generator) predicts the action a , *i.e.*, the configuration for the next camera (Eq. 1 and Eq. 3). On the right, the environment (simulation engine and detector) takes the predicted camera configurations and feeds rendered images to the multi-view pedestrian detector. It returns the list of configurations for existing cameras as the state s (Eq. 2), and the detection accuracy as the reward r (Eq. 4). Dotted lines denote non-differentiable operations.

for single image depth estimation, structured illumination for active depth estimation [2], point spread function (response to a point source of light) [6, 52] LiDAR pulse configuration [16] for detection, and optic components for HDR imaging [34, 46].

Reinforcement learning (RL) guides an agent to maximize cumulative rewards while interacting with the environment. RL is usually modelled as a Markovian Decision Process (MDP), characterized by the state s , the action a , the internal transition $P_a(s, s')$ from state s to state s' after taking action a , and the reward r . The goal of reinforcement learning is to learn a policy $\pi(a|s)$ that maximizes the expected cumulative reward. To learn the best policy, value-based methods like Q-learning and DQN [36] optimize the action value function $Q(s, a)$, which describes the estimated future return for a specific action a at state s . Policy gradient methods like REINFORCE [56] and PPO [44] directly optimize for the policy $\pi(a|s)$. RL has seen a wide adoption in many computer vision tasks. Specifically, researchers in neural architecture search also adopt RL to search neural network configurations that can give the best accuracy on validation sets [39, 61], which is comparable to our search of camera configuration.

3. Methodology

3.1. Problem Formulation

To investigate camera configuration generation for multi-view pedestrian detection, we consider an interactive formulation. As shown in Fig. 2, on the left, the *agent*, camera configuration generator $g(\cdot)$ predicts camera configuration as its action a . On the right, the *environment* takes as input the action (camera configuration), renders images, and feeds the images to the detection network $f(\cdot)$. Finally, it returns the detection accuracy as reward r and considers the updated camera configuration as state s . It is noteworthy that, unlike most environments, the detection network can also be jointly trained, resulting in non-static rewards throughout the search process.

Mathematically, we define the configuration $c \in \mathbb{R}^7$ for

a camera as a 7-dimensional vector,

$$c = (x, y, z, \cos \psi, \sin \psi, \theta, \alpha), \quad (1)$$

where x, y, z denotes the 3D location for the camera, ψ and θ denote the camera yaw and pitch angle, and α denotes the camera FoV. Note that in the configuration c , we use the cosine and sine values for the yaw angle $\psi \in [0, 2\pi]$ to avoid having two different values (0 and 2π) for the same angle [59]. The camera configuration c can be fed into the simulation engine to render a camera view x .

In our interactive formulation, we consider the sequential generation of configurations for N cameras. At a specific time step $t \in \{0, \dots, N-1\}$, there are t cameras whose configurations are already decided. For Markovian modelling, we represent the state s as,

$$s_t = \begin{cases} \emptyset, & \text{if } t = 0 \\ (c_1, \dots, c_t), & \text{otherwise} \end{cases}, \quad (2)$$

where \emptyset denotes an empty set. The action a taken at this time step determines the configuration for the next camera,

$$a_t = c_{t+1}. \quad (3)$$

And the reward r for each time step is set as,

$$r_t = \begin{cases} 0, & \text{if } t < N-1 \\ \text{MODA}(f(x_1, \dots, x_N), \mathbf{y}), & \text{otherwise} \end{cases}, \quad (4)$$

where $\text{MODA}(\cdot, \cdot)$ denotes the Multi-Object Detection Accuracy [27], the primary metric for multi-view pedestrian evaluation [7, 22]; $f(\cdot)$ denotes the multi-view pedestrian detection network; x_1, \dots, x_N are the rendered camera views from N cameras; and \mathbf{y} is the corresponding ground truth 3D locations for pedestrians.

3.2. CarlaX Environment

In order to investigate how effective different camera configurations are quantitatively, we need a dedicated testbed. Existing datasets on multi-view detection like Wildtrack [7]

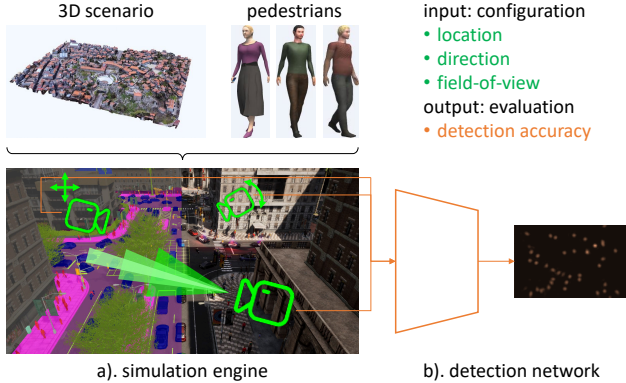


Figure 3. The interactive environment has two main components for controllable camera rendering and evaluation: a). the simulation engine and b). the multi-view pedestrian detection network. Given configurations, the simulation renders camera views, which are then fed into the detection network for quantitative evaluation.

and MultiviewX [22] only contain static images collected from expert-designed camera rigs. To fill in the gap of controllable camera rendering and evaluation, an interactive simulation environment, CarlaX, is introduced in this work.

CarlaX connects the autonomous driving engine, Carla [12], with the multi-view pedestrian detection network (see Fig. 3). The *simulation engine* takes as input the camera configurations, which include the 3D location x, y, z , the camera yaw angle ψ and pitch angle θ , plus the camera FoV α . Next, it renders the image for the 3D scenario and randomly populated pedestrians. Corresponding ground truth for 3D human locations is also preserved for further evaluation of the detection model. The multi-view pedestrian *detection network* $f(\cdot)$ then takes the rendered image views and estimates the 3D locations for pedestrians, which are then compared with the ground truth for evaluation.

3.3. Camera Configuration Generation

It is our goal to learn a policy network $g(\cdot)$ that can predict camera configurations based on the sequential state representation in Eq. 2. Importantly, the prediction for the next camera’s configuration should be *invariant* to the specific sequential order of the previous camera configurations, *e.g.*, for $t = 2$, $s_2 = (c_1, c_2)$, the policy for the next action $\pi(a_2 | (c_1, c_2)) = \pi(a_2 | (c_2, c_1))$.

To make the policy $\pi(a|s)$ *invariant* to the sequence order, we adopt the transformer architecture [53]. Unlike fully connected layers where the concatenation order of the state tokens can affect its results, self-attention operations in transformers are *permutation invariant*, making it ideal for our usage. The overall architecture is demonstrated in Fig. 4. Specifically, we only adopt the encoder part of the transformer to avoid excessive parameters and overfitting. We also maintain N embedding as configuration prediction

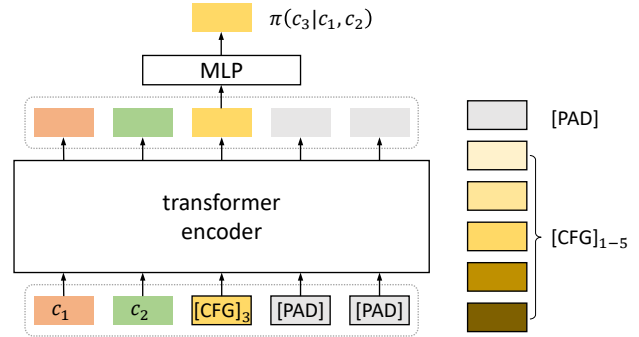


Figure 4. Architecture for camera configuration generator. For a time step $t = 2$ when configuring a total $N = 5$ cameras, we feed a fixed length input into the transformer encoder, consisting of configurations c_1 and c_2 for the first two cameras, a specific prediction token $[CFG]_3$ for the third camera, and two padding tokens $[PAD]$. Only the output for the prediction token $[CFG]_3$ is then fed into a multi-layer perceptron (MLP) to estimate the action for this time step $a_2 = c_3$, which is the configuration for the third camera. Solid black borders indicate learnable parameters.

tokens $\{[CFG]_1, \dots, [CFG]_N\}$ and a padding token $[PAD]$.

The forward pass of the network is depicted as follows,

$$\pi(a_t | s_t) = g(s_t, [CFG]_{t+1}, [PAD]). \quad (5)$$

At a specific time step $t \in \{0, \dots, N - 1\}$, given existing t camera configurations in the state vector s_t , we append a specific prediction token $[CFG]_{t+1}$ and pad the sequence into a total of N tokens. No positional embedding is used to maintain the permutation invariant property. The transformer encoder output for the prediction token $[CFG]_{t+1}$ is then fed into a multi-layer perceptron (MLP) to estimate the policy $\pi(a_t | s_t)$.

3.4. Training Scheme

In order to effectively navigate the vast action space while dealing with non-differentiable procedures in the interactive environment, we use reinforcement learning to guide the camera configuration policy. Specifically, we adopt the PPO algorithm [44], a policy-gradient-based RL method for its simplicity and stability. After collecting a buffer of state s , action a , and reward r , PPO estimates the specific advantage [43] for taking an action, and updates the policy network $g(\cdot)$ using its policy loss. During the camera search process, the detection network can also be jointly trained using the ground truth pedestrian locations. We show a step-by-step training scheme in Algorithm 1.

Despite the effectiveness of the PPO algorithm, the policy gradient remains a little indirect compared to differentiable feedback. This can be potentially problematic considering the vast action space – for each camera, the action space spans over $>1000\text{m}^3$ for camera location, 2π for the

Algorithm 1 Training scheme for the proposed method.

```

1: input: camera configuration generator  $g(\cdot)$ , detection network  $f(\cdot)$ , number of cameras  $N$ , PPO buffer size  $L$ , maximum steps  $T$ .
2: initialize iteration counter  $i = 0$  and PPO buffer  $B = \emptyset$ ;
3: while  $i < T$  do
4:   randomly populate pedestrians in the simulation scenario;
5:   initialize the state  $s_0 = \emptyset$ ;
6:   for time step  $t \in \{0, \dots, N - 1\}$  do
7:     select action  $a_t = \mathbf{c}_{t+1} \sim \pi(a_t | s_t)$  using  $g(\cdot)$ ;
8:     spawn the next camera and render its view  $\mathbf{x}_{t+1}$ ;
9:     if  $t < N - 1$  then
10:      set  $r_t = 0$ ;
11:     else
12:      calculate detection result  $\tilde{\mathbf{y}} = f(\mathbf{x}_1, \dots, \mathbf{x}_N)$  and set  $r_t = \text{MODA}(\tilde{\mathbf{y}}, \mathbf{y})$ ;
13:      calculate detection loss and optimize  $f(\cdot)$ ;
14:     end if
15:     update the PPO buffer  $B = B \cup \{s_t, a_t, r_t\}$ ;
16:     calculate the next state  $s_{t+1} = s_t \cup \{\mathbf{c}_{t+1}\}$ ;
17:     update the iteration counter  $i = i + 1$ ;
18:   end for
19:   if  $|B| > L$  then
20:     calculate PPO loss, the two regularization terms  $R_{\text{diverse}}$  and  $R_{\text{focus}}$ , and optimize  $g(\cdot)$ ;
21:     set the PPO buffer  $B = \emptyset$ ;
22:   end if
23: end while
24: return: configuration generator  $g(\cdot)$  and detector  $f(\cdot)$ .

```

camera yaw angle, plus the pitch angle and camera FoV. In this case, we introduce two additional heuristic-based regularization terms for the camera configurations, both of which can provide direct and differentiable supervision.

Our first heuristic is that cameras should ideally be diverse in their viewing angles. Mathematically, we compute the diversity regularization term as,

$$R_{\text{diverse}} = - \sum_{\tau} \|\bar{x} - \bar{x}_{\tau}, \bar{y} - \bar{y}_{\tau}\|_2 - \sum_{\tau} \|(\cos \psi - \cos \psi_{\tau}, \sin \psi - \sin \psi_{\tau})\|_2, \quad (6)$$

where τ denotes a total of t previous cameras. By minimizing this regularization term, cameras are encouraged to provide different viewing angles.

Our second heuristic is that cameras should focus on the scenario and avoid looking outside of the scenario. For the regularization term, we consider the following,

$$R_{\text{focus}} = \frac{\|(\bar{x} + \delta \cos \psi, \bar{y} + \delta \sin \psi)\|_2 - \|(\bar{x}, \bar{y})\|_2}{\delta}, \quad (7)$$

where $\|\cdot\|_2$ denotes the Euclidean norm; $\bar{x}, \bar{y} \in [-1, 1]$ are normalized camera xy coordinates; δ is a small hyperparameter. Promoting a smaller regularization term R_{focus}

Table 1. Datasets comparison for multi-view pedestrian detection.

	#camera	frames	area	#person
Wildtrack	7	400	$12 \times 36 \text{ m}^2$	20
MultiviewX	6	400	$16 \times 25 \text{ m}^2$	40
CarlaX	up to 6	400	up to $45 \times 39 \text{ m}^2$	up to 80

can penalize camera yaw angle ψ for looking outside of the scenario when the positioning is already offset to that side.

4. Experiment

4.1. Experimental Settings

Camera parameters and action space. In our study, we consider basic RGB cameras that can be mounted at a specific location and direction with a fixed focal length. In terms of the action space for camera configurations (Eq. 1), the range for location x, y, z is determined by specific scenarios; the yaw angle $\psi \in [0, 360^\circ]$ spans the entire unit circle; the pitch angle $\theta \in [-30^\circ, 30^\circ]$ allows the camera to adjust for different mounting height; and the FoV $\alpha \in [30^\circ, 120^\circ]$ covers the common focal lengths [54].

Simulation scenarios. We introduce seven distinct scenarios in our interactive environment, CarlaX. An overall statistical comparison between CarlaX and existing datasets Wildtrack [7] and MultiviewX [22] can be found in Table 1. By default, in each scene, we randomly populate up to 40 walking people and up to 10 groups of 2 to 4 chatting persons. Although CarlaX can generate infinite pedestrian distributions, we limit them to 400 distinct patterns (frames) to mimic existing datasets.

- Town03cafe: a small coffee shop with tables, located in the middle of four apartment buildings.
- Town03park: a park with trees, slopes, swings, and a lot of open space, making it difficult to cover.
- Town04building: a plaza between buildings with occlusions from a pergola (sitting area with pillars supporting an open lattice top) and sunshades of street shops.
- Town04crossroad: a crossroad with traffic lights. It is very open and easy for pedestrian detection.
- Town05building: a plaza between buildings but without severe occlusions.
- Town05market: the most challenging scenario, covering a flea market with multiple rows of shops and food stands.
- Town05skyscraper: an area between high buildings with a giant tree, limiting visibility from certain angles.

As shown in Table 2, each scene has a different Degree of Freedom (DoF) for the camera location (x, y, z in camera configuration c) and pedestrian spawning (only two out of three dimensions). Specifically, due to the nature of the scenario, we set different ranges for the camera mounting height (z), since tall buildings can naturally support higher

Table 2. Detection performance comparison on seven CarlaX scenarios. We compare the proposed method with three human experts, random search, and maximum FoV coverage, under various numbers of cameras and location Degrees of Freedom (DoFs). The results of three optimization-based methods are the average of 5 independent runs with standard deviation. MODA (%) is reported. The best results are shown in **bold**. Our proposed approach is better than the best human configuration.

Scenario	#camera	Location DoF	Camera configuration designs					
			Expert 1	Expert 2	Expert 3	random search	max coverage	proposed
Town03cafe	4	$42 \times 10 \times 6 \text{ m}^3$	71.3	85.8	77.4	25.9 ± 10.2	60.7 ± 3.0	91.7 ± 0.7
Town03park	3	$45 \times 39 \times 7 \text{ m}^3$	69.9	82.6	70.0	57.4 ± 5.0	65.4 ± 2.7	92.0 ± 0.5
Town04building	4	$15 \times 30 \times 8 \text{ m}^3$	72.4	89.0	82.9	46.3 ± 7.0	52.1 ± 4.4	95.8 ± 0.4
Town04crossroad	4	$20 \times 20 \times 4 \text{ m}^3$	95.3	94.2	95.0	90.2 ± 4.4	74.4 ± 2.2	98.6 ± 0.2
Town05building	4	$15 \times 25 \times 8 \text{ m}^3$	91.2	94.4	72.9	66.5 ± 6.3	76.5 ± 1.9	98.5 ± 0.2
Town05market	6	$56 \times 22 \times 4 \text{ m}^3$	48.1	58.6	44.3	21.3 ± 4.2	15.3 ± 3.9	68.7 ± 1.5
Town05skyscraper	3	$28 \times 11 \times 6 \text{ m}^3$	92.9	90.4	85.2	72.9 ± 6.9	79.0 ± 1.9	97.9 ± 0.1

mounting points while newspaper stands and flea markets cannot support very high mounting points.

Baselines considered in this study are listed as follows.

- *Human expert*: we recruit three human experts to position the cameras for each scenario.
- *Random search*: a similar computation budget is given to randomly generate camera configurations, and *greedily* chooses the configuration that gives the best detection accuracy on one frame of training images.
- *Maximum FoV coverage*: following previous works [14, 49], we consider the FoV coverage of ground plane building floor plans as a heuristic for camera placement study. During training, we follow previous work and do not spawn pedestrians into the scenario, so as to focus on the occlusion introduced by the static objects like tables, chairs, trees, buildings, *etc.* The configuration with the highest FoV coverage for the ground plane is selected.

We do not consider view selection methods for 3D reconstruction [15, 31, 58], since they serve a very different purpose (recognition of foreground objects v.s. reconstruction of static background) and often require hundreds of views.

Multi-view pedestrian detection network. We choose MVDet [22] as the detector network $f(\cdot)$ in this study, but it can be changed into more advanced architectures like SHOT [47] or MVDeTr [21].

Evaluation metric. Evaluation metrics for multi-view pedestrian detection include multi-object detection accuracy (MODA, the primary indicator), multi-object detection precision (MODP, evaluation for localization error), and precision and recall (combined they give MODA) [27]. Following previous work [21, 22, 47], we consider MODA as the primary indicator for performance, since detecting the targets (MODA, precision, recall) is more important than having the most accurate localization (MODP), and MODA accounts for both precision and recall.

4.2. Implementation Details

For our camera configuration generator, we use three layers of transformer encoder with a feature dimension of 128.

We train all networks for 50 epochs (which roughly gives $T = 50,000$ training steps when there are three cameras in the scene) using the Adam optimizer [29]. We use learning rates of 1×10^{-5} and 1×10^{-4} for $f(\cdot)$ and $g(\cdot)$, respectively. For the PPO training, we use a buffer size of $L = 1024$ and a mini-batch size of 128, and train on each recorded experience 10 times. Regarding hyperparameters, we set the weight for the two regularization terms as 0.1.

All experiments are run on one RTX-3090 GPU and averaged across 5 repetitive runs, taking roughly 8 hours each.

4.3. Experimental Results

We compare the multi-view pedestrian detection performance in Table 2 and Fig. 5. Overall, we find the proposed method consistently outperforms the human experts and baseline methods. We have the following findings.

First, we find that different *human experts* achieve quite diverse performance (Table 2) due to their distinct preferences (Fig. 5): Expert 1 tends to position cameras along the sides; Expert 2 likes to position cameras at the corners of the scenario; Expert 3 combines close-up views with wide-angle views, possibly reflecting some conscious or unconscious bias or preferences. Arguably, these expert configurations all make sense, but which of them actually yields the best results requires experimental verification, something often overlooked in human expert designs [10, 20, 54, 60]. This also verifies the need for an interactive playground to import 3D scene scanning and quantitatively test out the detection accuracy of the potential configurations, something we provide in our CarlaX environment.

Second, we find that *random search* cannot efficiently locate the helpful views and is very noisy. In fact, with multiple experiments showing test accuracy first increasing and then decreasing, we find the detection accuracy on one frame of training images is not a very robust indicator, as the test set might display rather different pedestrian distributions. Also, the large variance between different repeats of random search (Table 2) indicates such simple approach is not suitable for vast action spaces.

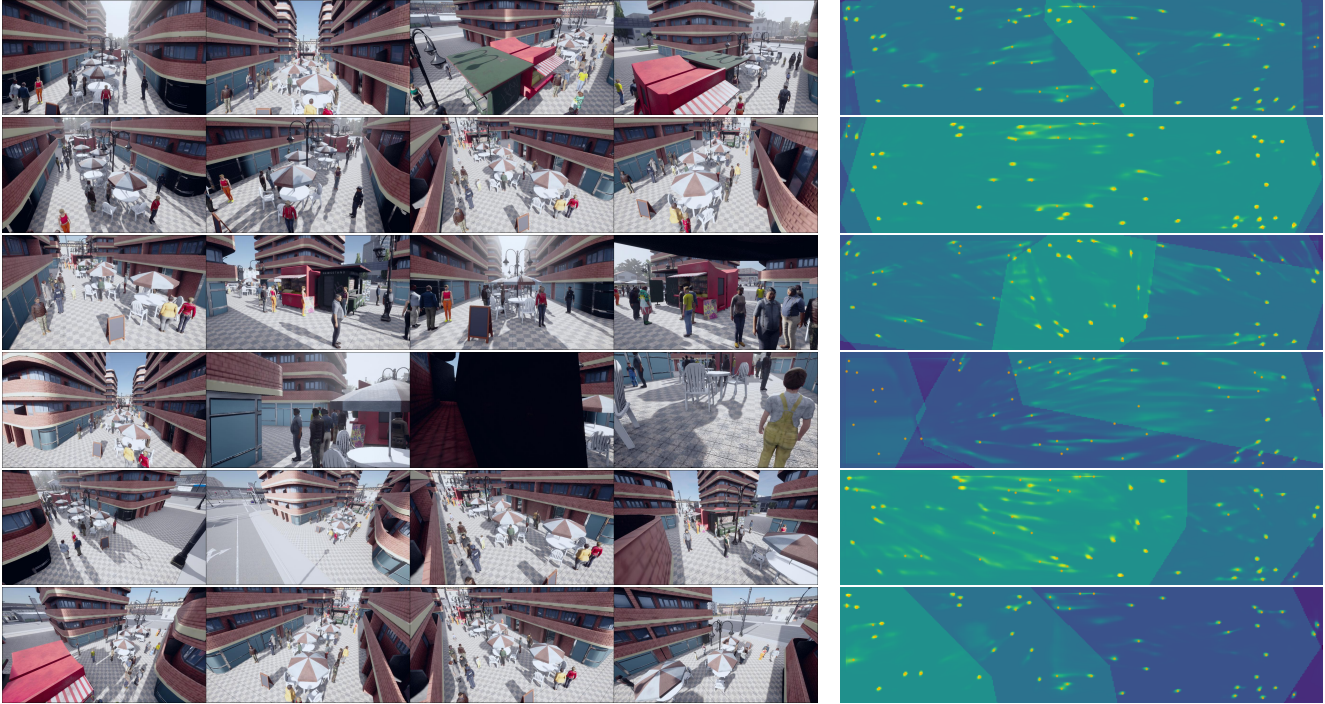
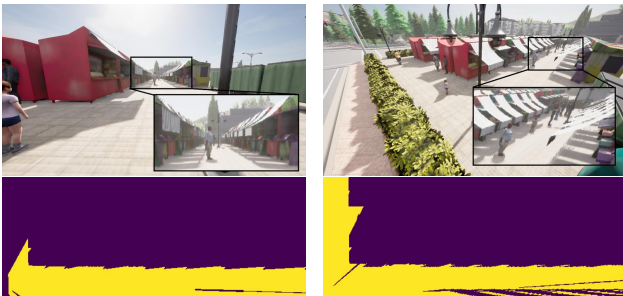


Figure 5. Comparison between camera configurations on `Town03cafe`. From top to bottom, we have camera views from Expert 1, Expert 2, Expert 3, random search, max coverage, and the proposed method. We also show FoV coverages and detection results (heatmap overlay) for pedestrians (orange dots). For more visualizations of other scenarios, please see the Appendix.



(a) Max FoV coverage

(b) Proposed method

Figure 6. Comparison on `Town05market`. Although (a) provides good coverage (bottom) of the aisle between shops, it struggles with occlusions introduced by pedestrians (top).

Third, we find that *maximum coverage* is a relatively good heuristic, but cannot consistently outperform human experts in terms of task performance (Table 2) when under vast action spaces. We demonstrate two views in Fig. 6, both of which provide similar FoV coverage when the scenario is empty. However, when the scene is populated, they offer different levels of help for detection under occlusion. Since FoV coverage maximization methods [14, 49] run the optimization in empty scenes (populating the scene will introduce random occlusions, which poses additional challenges for the optimization process), it is difficult for them

to guarantee good detection accuracy under occlusion.

Last but not least, the proposed optimization can steadily converge 7 and demonstrates consistent performance across multiple scenarios. It learns complex strategies, including maximizing FoV coverage, selecting diverse viewpoints, minimizing the occlusion from both static scenes (*e.g.*, the sunshade in Fig. 5) and other pedestrians, and collaborating with other cameras. Compared to human experts, it also shows to be the most advantages in the most challenging scenario with most cameras, *i.e.*, +10.1% MODA in `Town05market`.

4.4. Discussions

Fixed detection network. As shown in Table 3, fixing the detector $f(\cdot)$ limits the overall system performance. However, under this setting, the RL search alone still achieves competitive performance to the best-performing human expert. Such results verify the effectiveness of both the RL search method itself, and the necessity of jointly training the detection network.

Choice of generator architecture. We find that using MLP for the camera configuration generator network $g(\cdot)$ results in worse performance (Table 3) due to the dependency on the configuration sequence order: during RL training, the agent might sample similar configurations in different orders, which are the same to the simulation rendering.

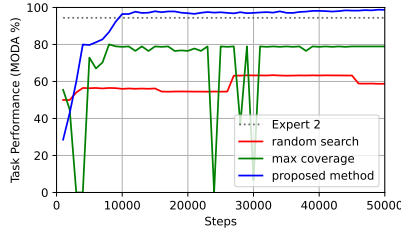
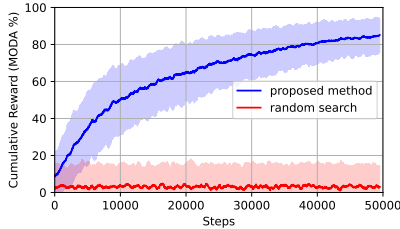


Figure 7. Convergence on Town05building. On the left, we show the cumulative reward of the training set MODA (max coverage [14, 49] uses floor plan coverage as reward, not MODA). On the right, we show the test set MODA for searched configurations.

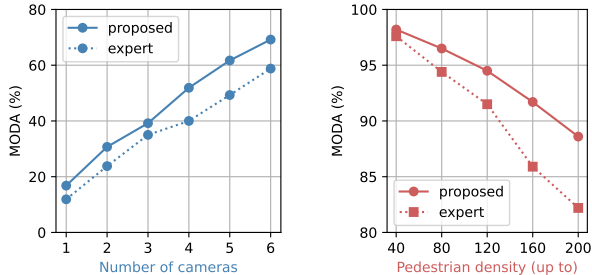


Figure 8. Performance scaling over different numbers of cameras (left, Town05market) and different pedestrian density (right, Town05building).

Directly concatenating the state vector s can result in two very different feature vectors $c_1 + c_2$ and $c_2 + c_1$, where $+$ denotes the concatenation operation, causing additional difficulties for training. The proposed transformer architecture (Section 3.3), on the other hand, is *permutation invariant* and thus easier to train.

Influence of the regularization terms. In Table 3, we find that removing either of the regularization terms leads to performance drops. In fact, compared to running the official PPO implementation [41] on classic RL environments like Atari [36] and Mujoco [51] for 2M steps, running the RL algorithm over 50k training steps is rather short. However, the complex simulation update in CarlaX makes more training steps very costly, and the differentiable approximation of policy gradient [50] is not the most efficient signal. Thus, having differentiable regularization terms (Section 3.4) that can filter out unlikely choices turns out to be quite handy.

Performance scaling. In Fig. 8, we show the system performance over different numbers of cameras and pedestrian density and compare them with the best human expert.

For the number of cameras, we find that using fewer cameras can be even more challenging for this scene since they cannot cover the entire area and have no other camera to collaborate with when dealing with occlusions. Increasing the number of cameras alleviates this issue, and the search method maintains its lead over the best human expert across different numbers of cameras.

For the pedestrian density, we find that not only does the proposed layout outperform the best human expert, but its

Table 3. Variant study. The MLP generator fails to converge on Town05building, denoted as Did Not Converge (DNC).

Variants	T03park	T05bldg
proposed method	92.0	98.5
fixed detector	83.9	97.1
MLP generator	36.8	DNC
w/o $R_{diverse}$	90.0	97.9
w/o R_{focus}	88.2	98.1

advantages grow even larger in more crowded scenes.

Additionally, from Table 2, we also find the proposed method to have bigger advantages over human experts in scenes that have more cameras (e.g., Town05market), more area (e.g., Town03park), or more occlusions (e.g., Town03cafe, Town04building, Town05market).

Generalization to the real world. For real-world applications, we can first scan the scenario into 3D with smartphones [1, 11, 37]; and then import the 3D scenario into CarlaX; and then jointly optimize both camera configurations and detection networks; and finally run domain adaptation algorithms [26, 28] for synthetic-to-real adaptation.

Limitation and ethics. In this work, we focus on multi-view pedestrian detection. Although this task touches multiple fronts including combating occlusions, reducing ambiguities, and increasing FoV coverage, it only focuses on pedestrians. In the future, we aim to extend this work to more classes like vehicles and to other tasks including 3D reconstruction. Moreover, we acknowledge that technologies like pedestrian detection can potentially have negative social impacts on privacy. To best avoid this issue, we conduct experiments on synthetic data. Plus, the searched camera configurations are usually from higher viewing angles (see Fig. 5 and Fig. 6), further alleviating privacy issues.

5. Conclusion

In this paper, we extend the optimization from neural network parameters to camera configurations, and study this problem under the challenging task of multi-view pedestrian detection. Unlike previous camera placement designs that either rely on human experts or heuristic-based surrogates, we directly optimize for the task performance. To this end, we introduced an interactive environment, CarlaX, which not only enables this work but also allows for future study on camera configurations. We also designed a transformer-based configuration generator and a reinforcement-learning-based training scheme, the combination of which helps design camera configurations that can give very competitive detection accuracy. Inspired by the success of this camera configuration study, we would like to extend the optimization to other fields, including 3D recon-

structions from hundreds of views and robotic vision where both camera angles and robot movements can be controlled.

References

- [1] Apple. iphone 14 pro and iphone 14 pro max. <https://www.apple.com/iphone-14-pro/>. 8
- [2] Seung-Hwan Baek and Felix Heide. Polka lines: Learning structured illumination and reconstruction for active stereo. In *Proceedings of the IEEE/CVF Conference on Computer Vision and Pattern Recognition*, pages 5757–5767, 2021. 3
- [3] Pierre Baqué, François Fleuret, and Pascal Fua. Deep occlusion reasoning for multi-camera multi-target detection. In *Proceedings of the IEEE International Conference on Computer Vision*, pages 271–279, 2017. 2
- [4] Holger Caesar, Varun Bankiti, Alex H Lang, Sourabh Vora, Venice Erin Liong, Qiang Xu, Anush Krishnan, Yu Pan, Giancarlo Baldan, and Oscar Beijbom. nuscenes: A multi-modal dataset for autonomous driving. In *Proceedings of the IEEE/CVF conference on computer vision and pattern recognition*, pages 11621–11631, 2020. 1
- [5] Ayan Chakrabarti. Learning sensor multiplexing design through back-propagation. *Advances in Neural Information Processing Systems*, 29, 2016. 2
- [6] Julie Chang and Gordon Wetzstein. Deep optics for monocular depth estimation and 3d object detection. In *Proceedings of the IEEE/CVF International Conference on Computer Vision*, pages 10193–10202, 2019. 3
- [7] Tatjana Chavdarova, Pierre Baqué, Stéphane Bouquet, Andrii Maksai, Cijo Jose, Timur Bagautdinov, Louis Lettry, Pascal Fua, Luc Van Gool, and François Fleuret. Wild-track: A multi-camera hd dataset for dense unscripted pedestrian detection. In *Proceedings of the IEEE Conference on Computer Vision and Pattern Recognition*, pages 5030–5039, 2018. 1, 3, 5
- [8] Tatjana Chavdarova et al. Deep multi-camera people detection. In *2017 16th IEEE International Conference on Machine Learning and Applications (ICMLA)*, pages 848–853. IEEE, 2017. 2
- [9] Shengyong Chen, Youfu Li, and Ngai Ming Kwok. Active vision in robotic systems: A survey of recent developments. *The International Journal of Robotics Research*, 30(11):1343–1377, 2011. 2
- [10] ConceptDraw. Camera layout schematic — security and access plans — how to create cctv network diagram — camera lay out. 1, 6
- [11] Andrew J Davison, Ian D Reid, Nicholas D Molton, and Olivier Stasse. Monoslam: Real-time single camera slam. *IEEE transactions on pattern analysis and machine intelligence*, 29(6):1052–1067, 2007. 8
- [12] Alexey Dosovitskiy, German Ros, Felipe Codevilla, Antonio Lopez, and Vladlen Koltun. Carla: An open urban driving simulator. In *Conference on robot learning*, pages 1–16. PMLR, 2017. 2, 4
- [13] Ugur Murat Erdem and Stan Sclaroff. Optimal placement of cameras in floorplans to satisfy task requirements and cost constraints. In *Omnivis2004, The fifth Workshop on Omnidirectional Vision, Camera Networks and Non-classical cameras*. Citeseer, 2004. 1, 2
- [14] Ugur Murat Erdem and Stan Sclaroff. Automated camera layout to satisfy task-specific and floor plan-specific coverage requirements. *Computer Vision and Image Understanding*, 103(3):156–169, 2006. 1, 2, 6, 7, 8
- [15] Xinyi Fan, Linguang Zhang, Benedict Brown, and Szymon Rusinkiewicz. Automated view and path planning for scalable multi-object 3d scanning. *ACM Transactions on Graphics (TOG)*, 35(6):1–13, 2016. 2, 6
- [16] Félix Goudreault, Dominik Scheuble, Mario Bijelic, Nicolas Robidoux, and Felix Heide. Lidar-in-the-loop hyperparameter optimization. In *Proceedings of the IEEE/CVF Conference on Computer Vision and Pattern Recognition*, pages 13404–13414, 2023. 3
- [17] Harel Haim, Shay Elmalem, Raja Giryes, Alex M Bronstein, and Emanuel Marom. Depth estimation from a single image using deep learned phase coded mask. *IEEE Transactions on Computational Imaging*, 4(3):298–310, 2018. 2
- [18] Abdullah Hamdi, Silvio Giancola, and Bernard Ghanem. Mvtn: Multi-view transformation network for 3d shape recognition. In *Proceedings of the IEEE/CVF International Conference on Computer Vision*, pages 1–11, 2021. 2
- [19] Lei He, Guanghui Wang, and Zhanyi Hu. Learning depth from single images with deep neural network embedding focal length. *IEEE Transactions on Image Processing*, 27(9):4676–4689, 2018. 2
- [20] Toshi Hori. Traffic camera system development. In *Real-Time Imaging II*, pages 81–90. SPIE, 1997. 1, 2, 6
- [21] Yunzhong Hou and Liang Zheng. Multiview detection with shadow transformer (and view-coherent data augmentation). In *Proceedings of the 29th ACM International Conference on Multimedia*, pages 1673–1682, 2021. 2, 6
- [22] Yunzhong Hou, Liang Zheng, and Stephen Gould. Multiview detection with feature perspective transformation. In *European Conference on Computer Vision*, pages 1–18. Springer, 2020. 1, 2, 3, 4, 5, 6
- [23] Yunzhong Hou, Zhongdao Wang, Shengjin Wang, and Liang Zheng. Adaptive affinity for associations in multi-target multi-camera tracking. *IEEE Transactions on Image Processing*, 31:612–622, 2021. 1
- [24] Yunzhong Hou, Stephen Gould, and Liang Zheng. Learning to select camera views: Efficient multiview understanding at few glances. *arXiv preprint arXiv:2303.06145*, 2023. 2
- [25] Junjie Huang, Guan Huang, Zheng Zhu, Yun Ye, and Dalong Du. Bevdet: High-performance multi-camera 3d object detection in bird-eye-view. *arXiv preprint arXiv:2112.11790*, 2021. 1
- [26] Naoto Inoue, Ryosuke Furuta, Toshihiko Yamasaki, and Kiyoharu Aizawa. Cross-domain weakly-supervised object detection through progressive domain adaptation. In *Proceedings of the IEEE conference on computer vision and pattern recognition*, pages 5001–5009, 2018. 8
- [27] Rangachar Kasturi, Dmitry Goldgof, Padmanabhan Soundararajan, Vasant Manohar, John Garofolo, Rachel Bowers, Matthew Boonstra, Valentina Korzhova, and Jing Zhang. Framework for performance evaluation of face, text,

- and vehicle detection and tracking in video: Data, metrics, and protocol. *IEEE Transactions on Pattern Analysis and Machine Intelligence*, 31(2):319–336, 2008. 3, 6
- [28] Mehran Khodabandeh, Arash Vahdat, Mani Ranjbar, and William G Mcready. A robust learning approach to domain adaptive object detection. In *Proceedings of the IEEE/CVF International Conference on Computer Vision*, pages 480–490, 2019. 8
- [29] Diederik P Kingma and Jimmy Ba. Adam: A method for stochastic optimization. In *ICLR (Poster)*, 2015. 6
- [30] Tzofi Klinghoffer, Kushagra Tiwary, Nikhil Behari, Bhavya Agrawalla, and Ramesh Raskar. Diser: Designing imaging systems with reinforcement learning. In *Proceedings of the IEEE/CVF International Conference on Computer Vision*, pages 23632–23642, 2023. 2
- [31] Soomin Lee, Le Chen, Jiahao Wang, Alexander Liniger, Suryansh Kumar, and Fisher Yu. Uncertainty guided policy for active robotic 3d reconstruction using neural radiance fields. *IEEE Robotics and Automation Letters*, 7(4):12070–12077, 2022. 2, 6
- [32] Zhiqi Li, Wenhai Wang, Hongyang Li, Enze Xie, Chonghao Sima, Tong Lu, Yu Qiao, and Jifeng Dai. Bevformer: Learning bird’s-eye-view representation from multi-camera images via spatiotemporal transformers. In *European conference on computer vision*, pages 1–18. Springer, 2022. 1
- [33] Yilin Liu, Liqiang Lin, Yue Hu, Ke Xie, Chi-Wing Fu, Hao Zhang, and Hui Huang. Learning reconstructability for drone aerial path planning. *ACM Transactions on Graphics (TOG)*, 41(6):1–17, 2022. 2
- [34] Christopher A Metzler, Hayato Ikoma, Yifan Peng, and Gordon Wetzstein. Deep optics for single-shot high-dynamic-range imaging. In *Proceedings of the IEEE/CVF Conference on Computer Vision and Pattern Recognition*, pages 1375–1385, 2020. 3
- [35] Ben Mildenhall, Pratul P Srinivasan, Matthew Tancik, Jonathan T Barron, Ravi Ramamoorthi, and Ren Ng. Nerf: Representing scenes as neural radiance fields for view synthesis. *Communications of the ACM*, 65(1):99–106, 2021. 2
- [36] Volodymyr Mnih, Koray Kavukcuoglu, David Silver, Alex Graves, Ioannis Antonoglou, Daan Wierstra, and Martin Riedmiller. Playing atari with deep reinforcement learning. *arXiv preprint arXiv:1312.5602*, 2013. 3, 8
- [37] Raul Mur-Artal, Jose Maria Martinez Montiel, and Juan D Tardos. Orb-slam: a versatile and accurate monocular slam system. *IEEE transactions on robotics*, 31(5):1147–1163, 2015. 8
- [38] Joseph O’rourke et al. *Art gallery theorems and algorithms*. Oxford University Press Oxford, 1987. 2
- [39] Hieu Pham, Melody Guan, Barret Zoph, Quoc Le, and Jeff Dean. Efficient neural architecture search via parameters sharing. In *International conference on machine learning*, pages 4095–4104. PMLR, 2018. 3
- [40] Charles R Qi, Hao Su, Matthias Nießner, Angela Dai, Mengyuan Yan, and Leonidas J Guibas. Volumetric and multi-view cnns for object classification on 3d data. In *Proceedings of the IEEE conference on computer vision and pattern recognition*, pages 5648–5656, 2016. 1
- [41] Antonin Raffin, Ashley Hill, Adam Gleave, Anssi Kanervisto, Maximilian Ernestus, and Noah Dormann. Stable-baselines3: Reliable reinforcement learning implementations. *Journal of Machine Learning Research*, 22(268):1–8, 2021. 8
- [42] Ergys Ristani, Francesco Solera, Roger Zou, Rita Cucchiara, and Carlo Tomasi. Performance measures and a data set for multi-target, multi-camera tracking. In *European conference on computer vision*, pages 17–35. Springer, 2016. 1
- [43] John Schulman, Philipp Moritz, Sergey Levine, Michael Jordan, and Pieter Abbeel. High-dimensional continuous control using generalized advantage estimation. *arXiv preprint arXiv:1506.02438*, 2015. 4
- [44] John Schulman, Filip Wolski, Prafulla Dhariwal, Alec Radford, and Oleg Klimov. Proximal policy optimization algorithms. *arXiv preprint arXiv:1707.06347*, 2017. 3, 4
- [45] Steven M Seitz, Brian Curless, James Diebel, Daniel Scharstein, and Richard Szeliski. A comparison and evaluation of multi-view stereo reconstruction algorithms. In *2006 IEEE computer society conference on computer vision and pattern recognition (CVPR’06)*, pages 519–528. IEEE, 2006. 1
- [46] Vincent Sitzmann, Steven Diamond, Yifan Peng, Xiong Dun, Stephen Boyd, Wolfgang Heidrich, Felix Heide, and Gordon Wetzstein. End-to-end optimization of optics and image processing for achromatic extended depth of field and super-resolution imaging. *ACM Transactions on Graphics (TOG)*, 37(4):1–13, 2018. 3
- [47] Liangchen Song, Jialian Wu, Ming Yang, Qian Zhang, Yuan Li, and Junsong Yuan. Stacked homography transformations for multi-view pedestrian detection. In *Proceedings of the IEEE/CVF International Conference on Computer Vision*, pages 6049–6057, 2021. 2, 6
- [48] Hang Su, Subhransu Maji, Evangelos Kalogerakis, and Erik Learned-Miller. Multi-view convolutional neural networks for 3d shape recognition. In *Proceedings of the IEEE international conference on computer vision*, pages 945–953, 2015. 1
- [49] Yifan Sun, Qixing Huang, Dun-Yu Hsiao, Li Guan, and Gang Hua. Learning view selection for 3d scenes. In *Proceedings of the IEEE/CVF Conference on Computer Vision and Pattern Recognition*, pages 14464–14473, 2021. 2, 6, 7, 8
- [50] Richard S Sutton and Andrew G Barto. *Reinforcement learning: An introduction*. MIT press, 2018. 8
- [51] Emanuel Todorov, Tom Erez, and Yuval Tassa. Mujoco: A physics engine for model-based control. In *2012 IEEE/RSJ international conference on intelligent robots and systems*, pages 5026–5033. IEEE, 2012. 8
- [52] Ethan Tseng, Ali Mosleh, Fahim Mannan, Karl St-Arnaud, Avinash Sharma, Yifan Peng, Alexander Braun, Derek Nowrouzezahrai, Jean-Francois Lalonde, and Felix Heide. Differentiable compound optics and processing pipeline optimization for end-to-end camera design. *ACM Transactions on Graphics (TOG)*, 40(2):1–19, 2021. 3
- [53] Ashish Vaswani, Noam Shazeer, Niki Parmar, Jakob Uszkoreit, Llion Jones, Aidan N Gomez, Ł ukasz Kaiser, and Illia

Appendix

- Polosukhin. Attention is all you need. In *Advances in Neural Information Processing Systems*. Curran Associates, Inc., 2017. 4
- [54] Aliza Vigderman and Gabe Turner. Where to place your home security camera, 2023. 1, 5, 6
- [55] Wikipedia. Art gallery problem, 2022. 2
- [56] Ronald J Williams. Simple statistical gradient-following algorithms for connectionist reinforcement learning. *Reinforcement learning*, pages 5–32, 1992. 3
- [57] Yao Yao, Zixin Luo, Shiwei Li, Tian Fang, and Long Quan. Mvsnet: Depth inference for unstructured multi-view stereo. In *Proceedings of the European conference on computer vision (ECCV)*, pages 767–783, 2018. 1
- [58] Xiaohui Zhou, Ke Xie, Kai Huang, Yilin Liu, Yang Zhou, Minglun Gong, and Hui Huang. Offsite aerial path planning for efficient urban scene reconstruction. *ACM Transactions on Graphics (TOG)*, 39(6):1–16, 2020. 2, 6
- [59] Yi Zhou, Connelly Barnes, Jingwan Lu, Jimei Yang, and Hao Li. On the continuity of rotation representations in neural networks. In *Proceedings of the IEEE/CVF Conference on Computer Vision and Pattern Recognition*, pages 5745–5753, 2019. 3
- [60] Weijia Zong, Zhouyi Wang, Qiang Xing, Junjie Zhu, Liuwei Wang, Kai Qin, Hemin Bai, Min Yu, and Zhendong Dai. The method of multi-camera layout in motion capture system for diverse small animals. *Applied Sciences*, 8(9):1562, 2018. 1, 2, 6
- [61] Barret Zoph and Quoc V Le. Neural architecture search with reinforcement learning. *arXiv preprint arXiv:1611.01578*, 2016. 3

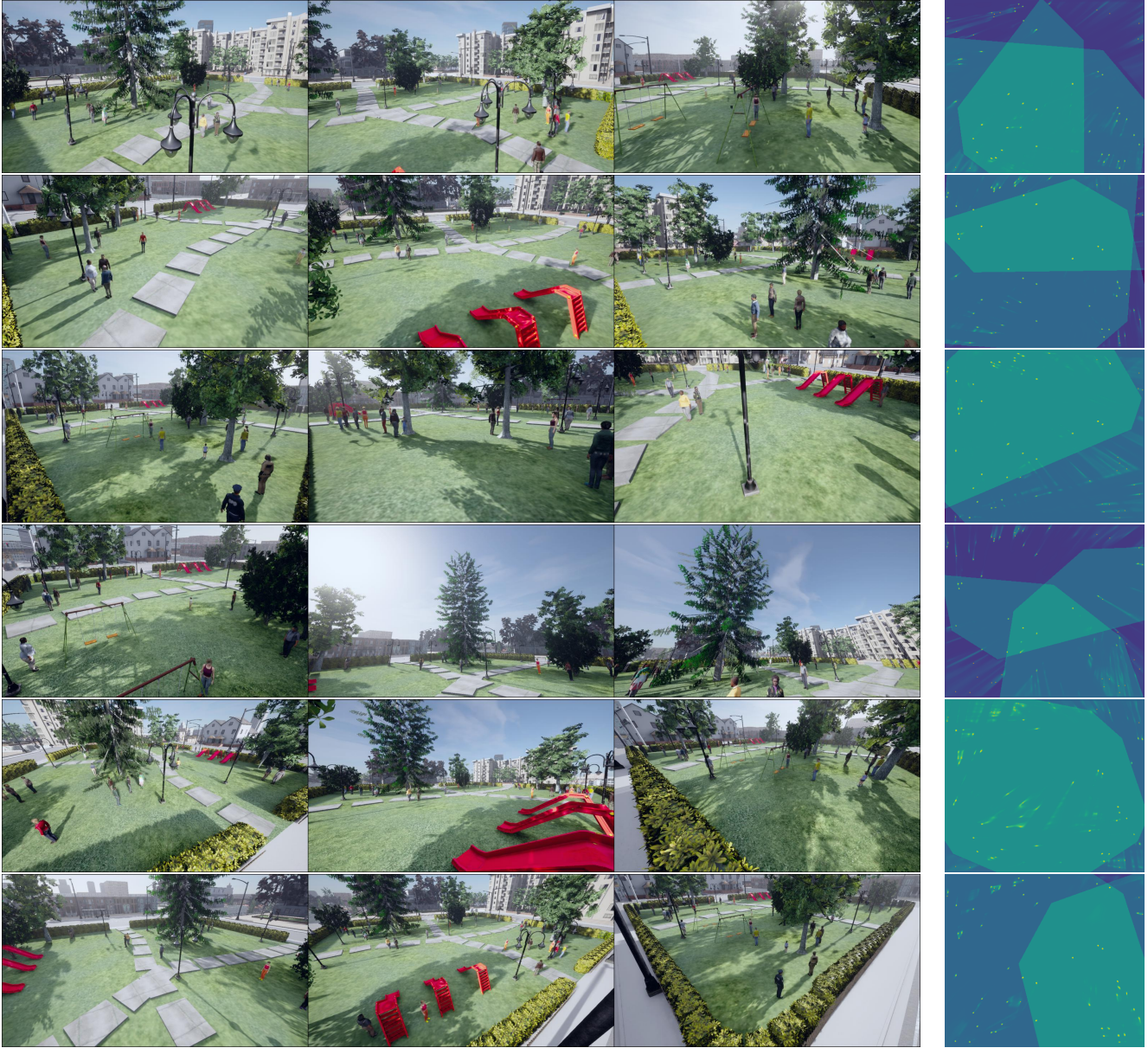


Figure 9. Comparison between camera configurations on Town03park. From top to bottom, we have camera views from Expert 1, Expert 2, Expert 3, random search, max coverage, and the proposed method. We also show FoV coverages and detection results (heatmap overlay) for pedestrians (orange dots).



Figure 10. Comparison between camera configurations on Town04building. From top to bottom, we have camera views from Expert 1, Expert 2, Expert 3, random search, max coverage, and the proposed method. We also show FoV coverages and detection results (heatmap overlay) for pedestrians (orange dots).



Figure 11. Comparison between camera configurations on Town04crossroad. From top to bottom, we have camera views from Expert 1, Expert 2, Expert 3, random search, max coverage, and the proposed method. We also show FoV coverages and detection results (heatmap overlay) for pedestrians (orange dots).

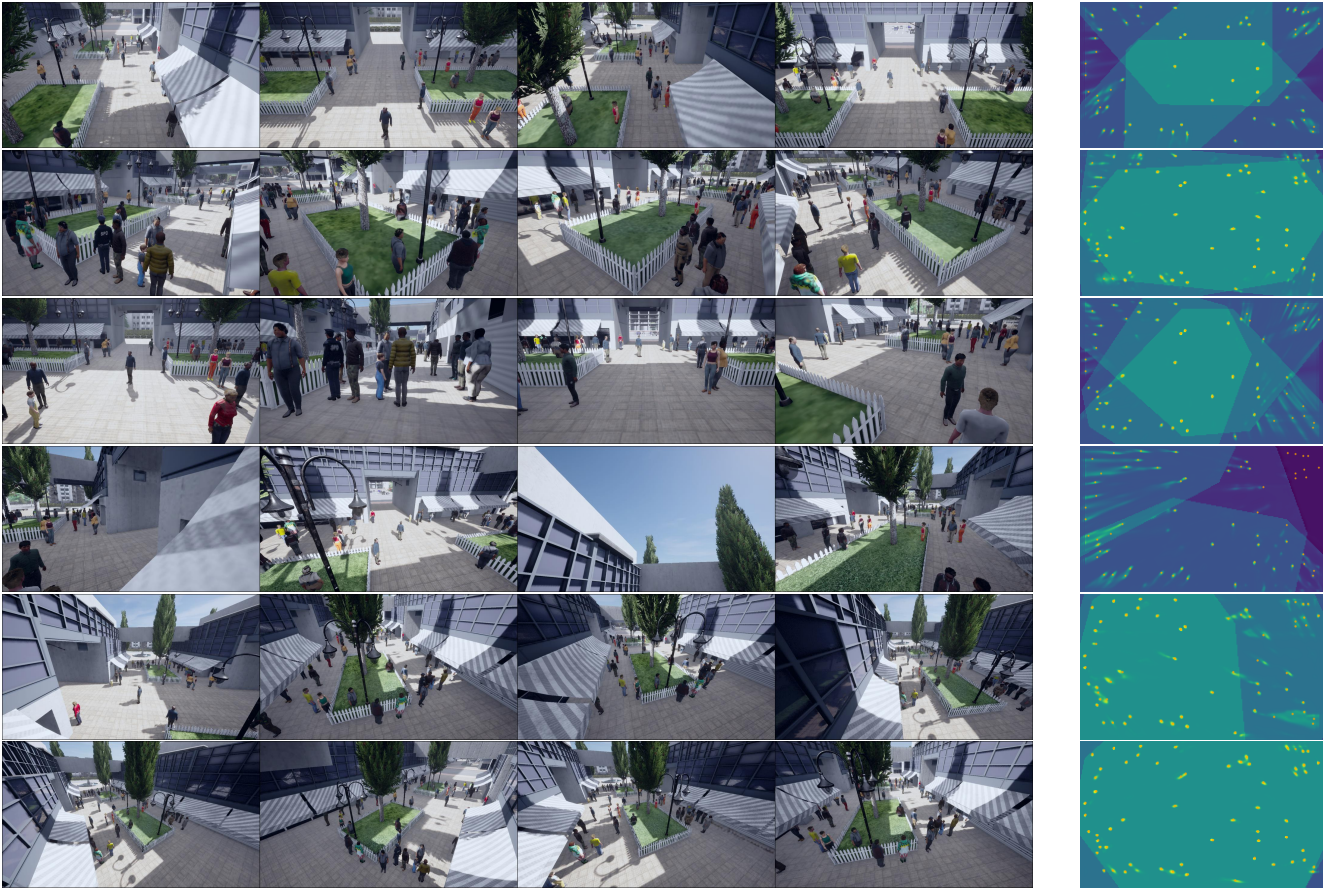


Figure 12. Comparison between camera configurations on Town05building. From top to bottom, we have camera views from Expert 1, Expert 2, Expert 3, random search, max coverage, and the proposed method. We also show FoV coverages and detection results (heatmap overlay) for pedestrians (orange dots).



Figure 13. Comparison between camera configurations on Town05market. From top to bottom, we have camera views from Expert 1, Expert 2, Expert 3, random search, max coverage, and the proposed method. We also show FoV coverages and detection results (heatmap overlay) for pedestrians (orange dots).

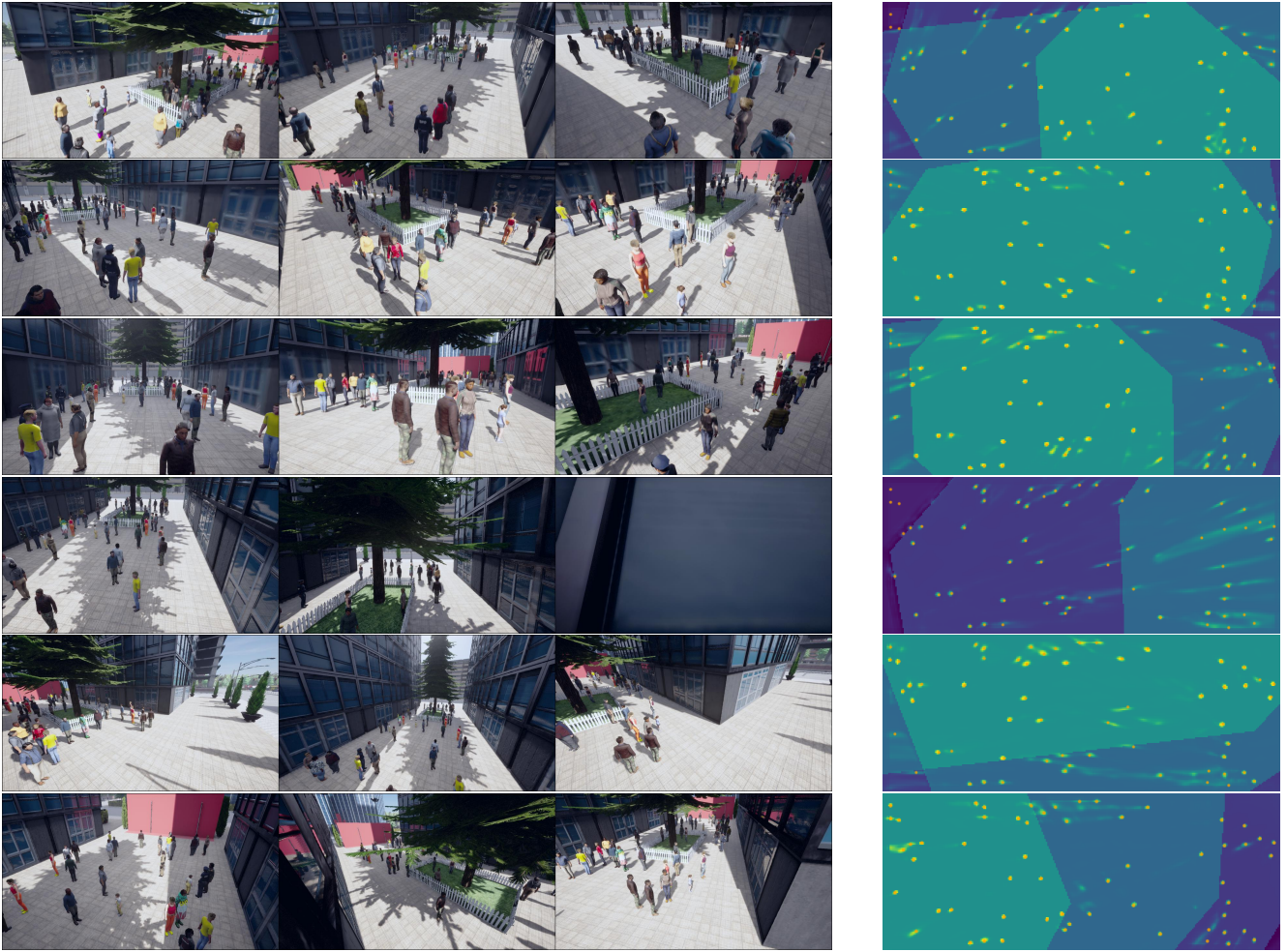


Figure 14. Comparison between camera configurations on `Town05skyscraper`. From top to bottom, we have camera views from Expert 1, Expert 2, Expert 3, random search, max coverage, and the proposed method. We also show FoV coverages and detection results (heatmap overlay) for pedestrians (orange dots).